# Osmotic concentration-controlled particle uptake and wrapping-induced lysis of cells and vesicles

Qingfen Yu<sup>1\*</sup>, Sabyasachi Dasgupta<sup>1,2\*\*</sup>, Thorsten Auth<sup>1</sup>, and Gerhard Gompper<sup>1</sup>

<sup>1</sup> Theoretical Soft Matter and Biophysics, Institute of Complex Systems and Institute for Advanced Simulation,

Forschungszentrum Jülich, D-52425 Jülich, Germany,

<sup>2</sup> Mechanobiology Institute, National University of Singapore, 11899 Singapore\*

In vivo, high solute and ion concentrations determine the preferred volumes of cells, organelles, and vesicles. Deformations of their lipid-bilayer membranes by nanoparticle wrapping reduce the interior volumes available to solutes and thus induce large osmotic pressure differences. Osmotic concentration can therefore be an important control parameter for wrapping of nanoparticles. We employ a curvature elasticity model of the membrane and contact interaction with spherical particles to study their wrapping at initially spherical vesicles. Whereas the continuous particle-binding transition is independent of the presence of solutes, the discontinuous envelopment transition shifts to higher adhesion strengths and the corresponding energy barrier increases with increasing osmotic concentration. High osmotic concentrations stabilize partial-wrapped, membrane-bound states for both, particle attachment to the inside and the outside. In this regime, wrapping of particles controls membrane tension—with power-law dependencies on osmotic concentration and adhesion strength. For high adhesion strengths, particle wrapping can lead to the opening of mechanosensitive channels in cell membranes and to lysis. Membrane tension-induced stabilisation of partial-wrapped states as well as wrapping-induced lysis play important roles not only for desired mechano-bacteriocidal effects of engineered nanomaterials, but may also determine viral burst sizes of bacteria and control endocytosis for mammalian cells.

 $\label{eq:Keywords: nanoparticles, osmotic pressure, membrane tension, endocytosis, mechano-bacteriocidal, mechanosensitive channels$ 

A large number of engineered nanoparticles can nowadays be fabricated with tuned physicochemical properties, such as size, shape, charge, and surface chemistry [1–5]. They are industrially used for various applications, e.g. in food and cosmetics industries, because of their large surface-to-volume ratio [6, 7]. Furthermore, a substantial amount of nano- and microplastics is found in oceans and seafood [8, 9]. A careful assessment of toxicological risks is thus essential [10, 11]. For potential applications in medical diagnostics and therapy, nanoparticles serve as markers for imaging [12–14], as heat sources for cancer therapy [15], and as vectors for targeted drug delivery [16, 17].

Small compartments bounded by lipid-bilayer membranes are essential for life: bacteria and eukaryotic cells are basic building blocks of life, organelles compartmentalise cells, and small vesicles can act as cargo containers. An important example is exosomes, small unilamellar vesicles that play important physiological roles in signalling and transport [18] and that can be used to detect cancer [19]. For systematic studies to advance both, predictive nanotoxicology and biomedical applications for nanomaterials, good control not only over membrane-nanoparticle interactions, but also over the physico-chemical properties of their environment is im-

portant [20, 21]. This is particularly evident for nanoparticle wrapping at vesicles. Figure 1 shows snapshots for the interaction between nanoparticles and vesicles in solutions with identical particle wrapping fractions and various solute-concentration differences of macromolecules or ions between the interior and the exterior. While the "neck" regions around the nanoparticles are catenoid-like for low osmotic concentrations, the overall shapes of the vesicles with partial-wrapped particles are more spherical for high osmotic concentrations. This indicates that in the latter systems, nanoparticle wrapping is controlled by osmotic pressure and induced membrane tension instead of membrane bending rigidity.

Biological systems usually contain high concentrations of ions and proteins, such that small volume changes of membrane-bounded compartments can induce large osmotic-pressure differences and large changes in membrane tension. Membrane tension is key for many internalization and secretion processes. For example, for a human erythroleukemia cell line, the endocytosis rate of fluorescent proteins has been shown to decrease with decreasing osmotic concentration in the external medium, and endocytosis is completely inhibited below a threshold value [22]. Internal stress of cells induced by adhesion to substrates can also suppress nanoparticle uptake [23, 24]. For bovine adrenal medullary cells, hypotonic and hypertonic extracellular solutions lead to increase and decrease of vesicular secretion, respectively [25]. Finally, under physiological conditions, the stiffness of adhered nanovesicles with sizes of about 100 nm is dominated by osmotic pressure rather than membrane bending energy [26].

<sup>\*</sup> Current address: Centre for Computational Science, Department of Chemistry, University College London, London WC1H 0AJ, United Kingdom

<sup>\*\*</sup> Current address: Department of Physics, University of Toronto, Toronto, Ontario M5S1A7, Canada

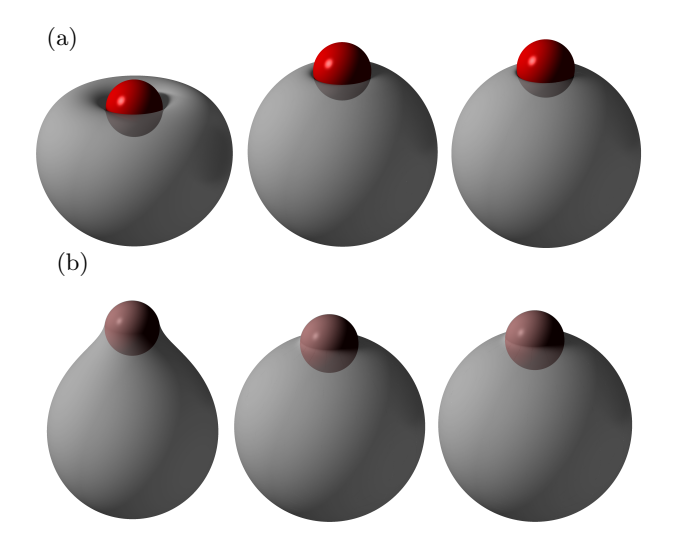


FIG. 1. Calculated shapes of initially pressureless spherical vesicles (gray) with fixed membrane area for (a) out-to-in and (b) in-to-out wrapping of spherical nanoparticles (red). The ratio of particle radius to vesicle radius is  $R_{\rm p}/R_{\rm v}=0.3$  and the wrapping fraction of the partial-wrapped particles is  $f_{\rm w}=0.41$ . The bending rigidity of the membrane is  $\kappa=50\,k_BT$ . From left to right the osmotic pressure difference between the vesicle and its surrounding increases; the snapshots belong to vesicles that contain  $\tilde{n}_{\rm v}=1,600$ ,  $\tilde{n}_{\rm v}=1.6\times10^6$ , and  $\tilde{n}_{\rm v}=1.6\times10^7$  entities of solute.

Implications of nanoparticle adhesion-induced membrane tension are crucial for signalling and toxicology. For example, MscS channels in E.coli open at a membrane tension  $\gamma=1.3\,k_BT/\mathrm{nm}^2$  [27] and MscL channels at  $\gamma=2.5\,k_BT/\mathrm{nm}^2$  [28, 29], such that a mechanical stimulus can induce an electrophysiological response. High membrane tension of embryonic stem cells can inhibit endocytosis of signalling components and thereby regulate their differentiation into specialized cells [30]. Finally, nanomaterials can act as antibacterials [31]. For example, nanoparticles can damage the cell walls of bacteria [32] and adhesion to natural and artificial nanostructured surfaces can induce membrane tension that leads to lysis of bacteria [33-35]—despite many bacteria are coated by liquid-crystalline lipopolysaccharide coats, so-called S-layers of proteins [36]. The existence of mechano-bacteriocidal activity is in particular supported by studies that use nanoparticles made from gold, which is a non-toxic material [37–39]. Along the same lines, nanomaterials are discussed as nanoantibiotics that do not suffer from the resistance development [40].

Deformation energies for fluid vesicles with or without particles have been calculated for various systems at vanishing osmotic concentration [41–44]. Here, we study the interaction of spherical particles with initially spherical vesicles in solutions with finite osmotic concentrations. We predict wrapping transitions between nonwrapped, partial-wrapped, and complete-wrapped states of the particles. In general, high osmotic concentrations stabilise partial-wrapped states. Furthermore, we calculate wrapping-induced membrane tensions and predict lysis of vesicles and opening of mechanosensitive channels of cells. For fixed particle-to-vesicle size ratio, the membrane tensions induced by partial-wrapped particles increase with increasing vesicle size, with increasing osmotic concentration, and with increasing adhesion strength. For lysis induced by many-particle adhesion, the number of particles required to reach the lytic tension of the membrane thus decreases with increasing adhesion strength. Lysis is facilitated by smaller vesicle sizes and larger particle sizes.

We employ a continuum membrane model to calculate membrane shapes and deformation energies. Continuum membrane models and energy minimisation have been successfully applied to predict interactions of fluid membranes with particles of different shapes and sizes [1]. The wrapping energy for a particle that interacts with a vesicle is the sum of the deformation energy costs and the adhesion energy gain,

$$E = 2\kappa \int_{A} dS H^{2} + E_{p} + \gamma_{L}A - w \int_{A_{ad}} dS, \qquad (1)$$

where  $\kappa$  is the bending rigidity and H the mean curvature of the membrane, w the adhesion strength between particle and membrane, A the total membrane area, and  $A_{\rm ad}$  the membrane area adhered to the particle. In addition, we take an osmotic pressure energy  $E_{\rm p}$  into account, as well as a term  $\gamma_{\rm L}A$  that fixes the total membrane area A of the vesicle, with the membrane tension  $\gamma_{\rm L}$  as Lagrange multiplier.

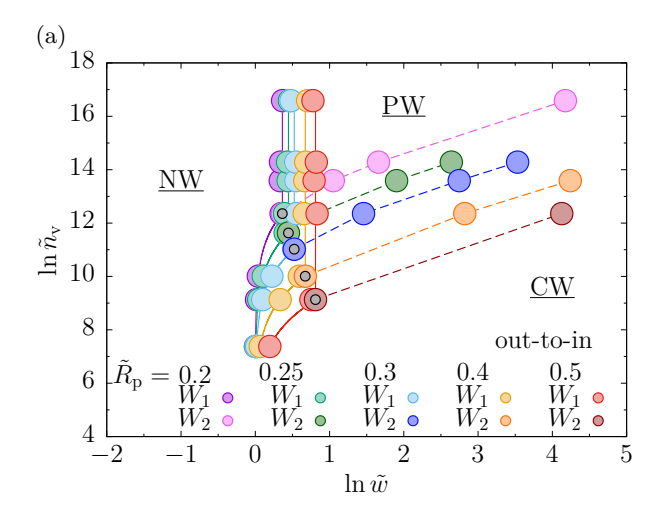
We consider an initially spherical vesicle with radius  $R_{\rm v}$  and volume  $V_0 = (4/3) \pi R_{\rm v}^3$ , and a spherical nanoparticle with radius  $R_{\rm p}$  and volume  $V_{\rm p} = (4/3) \pi R_{\rm p}^3$  suspended in buffer solution. Prior to wrapping, the overall osmotic concentration  $c_{\rm b} = n_{\rm b}/V_{\rm b}$  with the chemical amount  $n_{\rm b}$  of solute (measured in mol) in the buffer volume  $V_{\rm b}$  equals the osmotic concentration  $c_{\rm v} = n_{\rm v}/V_0$  in the interior of the vesicle with chemical amount  $n_{\rm v}$  of solute enclosed by the vesicle and the initial vesicle volume  $V_0$ . The osmotic pressure difference

$$\Delta\Pi = (c_{\rm v} - c_{\rm b}) N_{\rm A} k_{\rm B}T \tag{2}$$

between the buffer inside and outside the vesicle that develops during wrapping is determined by van't Hoff's formula, where  $N_{\rm A}=6.02\times 10^{23}\,{\rm mol}^{-1}$  is the Avogadro constant. During particle uptake, an initially spherical vesicle with v=1 assumes shapes with reduced volumes  $v=V/V_0<1$ . Therefore, the initially vanishing osmotic pressure difference increases and nanoparticle wrapping gets increasingly difficult with increasing particle wrapping fraction. By integrating over the pressure difference for the volume change from the spherical to the deformed state, we find the osmotic pressure energy

$$E_{\mathrm{p}}^{\mathrm{out2in}}(v) = \tilde{n}_{\mathrm{v}}(v - \ln v - 1) k_{\mathrm{B}}T \tag{3}$$

for  $\tilde{n}_{\rm v}=n_{\rm v}\,N_{\rm A}$  entities of solute in the vesicle, see supporting information. An analogous expression holds for



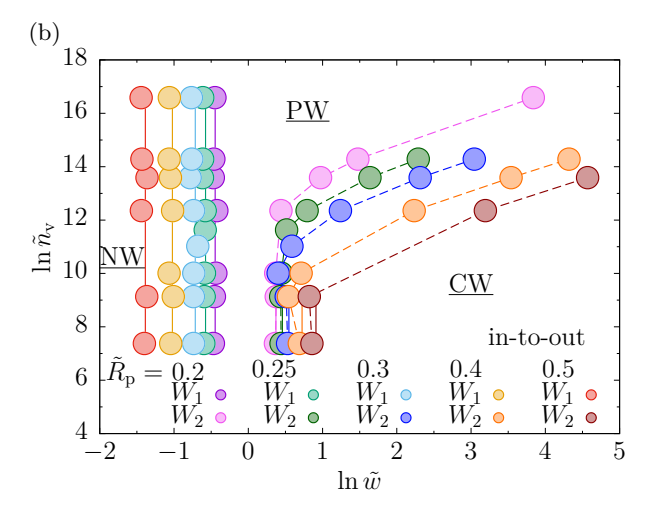


FIG. 2. Wrapping diagrams for (a) out-to-in and (b) in-to-out wrapping for various reduced adhesion strengths  $\tilde{w}$ , reduced osmotic concentrations  $\tilde{n}_{\text{V}}$ , reduced particle sizes  $0.2 \leq \tilde{R}_{\text{p}} \leq 0.5$ , and membrane bending rigidity  $\kappa = 50\,k_BT$ . Stable non-wrapped (NW), partial-wrapped (PW) and complete-wrapped (CW) states are separated by the binding or the binding-envelopment transition (NW-PW and NW-CW, both labeled as  $W_1$ ), and the envelopment transition (PW-CW, labeled as  $W_2$ ). The osmotic concentration-independent solid lines are the analytical predictions for the continuous transitions for the solute-free system from Ref. [45],  $\tilde{w} = (1 + \tilde{R}_{\text{p}})^2$  for out-to-in binding and  $\tilde{w} = (1 - \tilde{R}_{\text{p}})^2$  for in-to-out envelopment. The solid line for  $\tilde{w} = 1 + k_B T/(8\pi\kappa) \left(v_{02\mathrm{i,cw}} - \ln v_{02\mathrm{i,cw}} - 1\right) \tilde{n}_{\text{V}}$  represents the discontinuous binding-envelopment transition for out-to-in wrapping, see supporting information. The black points mark the analytically predicted triple points for out-to-in wrapping at  $\tilde{w}^* = (1 - \tilde{R}_{\text{p}})^2$  and  $\tilde{n}_v^* = 8\pi\kappa[(1 + \tilde{R}_{\text{p}})^2 - 1]/(v - \ln v - 1)$ . The dashed lines are guides to the eye for the numerical data.

a particle exiting a spherical vesicle with the effective reduced volume  $v^* = (V - V_{\rm p})/(V_0 - V_{\rm p})$ .

Experimental values for the number  $\tilde{n}_{\rm v}$  of entities of solute span a broad range  $0 < \tilde{n}_{\rm v} < 10^{13}$  [46–48]. Normal saline with 9 g of salt per liter and an osmotic concentration of 308 mOsm/l is almost isotonic. Under these physiological conditions,  $\tilde{n}_{\rm v} = 6 \times 10^4$  for a small vesicle with  $R_{\rm v} \approx 20$  nm,  $\tilde{n}_{\rm v} = 6 \times 10^7$  for a vesicle with  $R_{\rm v} \approx 20$  nm, and  $\tilde{n}_{\rm v} = 6 \times 10^{10}$  for a vesicle with  $R_{\rm v} \approx 2\,\mu{\rm m}$ . In the following, we use the reduced energy  $\tilde{E} = E/(8\pi\kappa)$ , the reduced adhesion strength  $\tilde{w} = wR_{\rm p}^2/(2\kappa)$ , and the particle-to-vesicle size ratio  $\tilde{R}_{\rm p} = R_{\rm p}/R_{\rm v}$ . The wrapping fraction is represented as  $f_{\rm w} = A_{\rm ad}/A_{\rm p}$ , where  $A_{\rm p}$  is the total surface area of the particle. Furthermore, we employ a reduced osmotic pressure for out-to-in wrapping,  $\Delta \tilde{\Pi} = \Delta \Pi R_{\rm v}^3/k_{\rm B}T$ .

Using triangulated surfaces [49–52], we calculate vesicle deformation energies for various wrapping fractions  $f_{\rm w}$ . Optimal vesicle shapes and minimal energies for fixed membrane area are obtained with the help of the freely available software package "Surface Evolver" [53]. Thermal membrane fluctuations are not taken into account in this approach. Such fluctuations have two main effects: (i) an excess membrane area stored in small-wavelength undulations, and (ii) a

short-ranged repulsion of nanoparticles [54]. Both effects are small for physiologically relevant bending rigidities,  $\kappa/(k_BT) > 10$ . Fluctuation contributions and vesicle deformation energies are discussed in more detail in the supporting information. Interestingly, for large particle-to-vesicle sizes and high osmotic pressure differences we find a wide-to-narrow neck shape transition. Particle wrapping is best characterized by wrapping diagrams that indicate the stable wrapping states for various adhesion strengths and osmotic concentrations. Figure 2 shows the wrapping transitions between non-wrapped and partial-wrapped  $(W_1)$ , non-wrapped and complete-wrapped  $(W_1)$ , and partial-wrapped and complete-wrapped states  $(W_2)$ . The wrapping transitions are obtained using the standard condition of equal wrapping energy  $E(w) = \min \left[ E(f_{w} - w f_{w}) \right]$  for coexisting states. [55, 56].

For out-to-in wrapping, an energy barrier separates the non-wrapped from complete-wrapped state [41–43, 45]. Therefore, for low osmotic concentrations, we find a combined binding-envelopment transition  $W_1$  from the non-wrapped to the complete-wrapped state in Fig. 2 (a), in agreement with the predictions for solute-free systems [41–43, 45]. With increasing osmotic concentration, the transition shifts to higher adhesion strengths,  $\tilde{w} = \tilde{n}_{\rm v} \, (v - \ln v - 1)/(8\pi\kappa) + 1$ , because the energetic costs for the volume change upon particle uptake increase, see supporting information. For high osmotic concentrations, partial-wrapped states are energetically favourable over the complete-wrapped state. All three

 $<sup>^1</sup>$  We vary the reduced particle radius  $\tilde{R}_{\rm p}$  by changing the vesicle radius  $R_{\rm v}.$ 

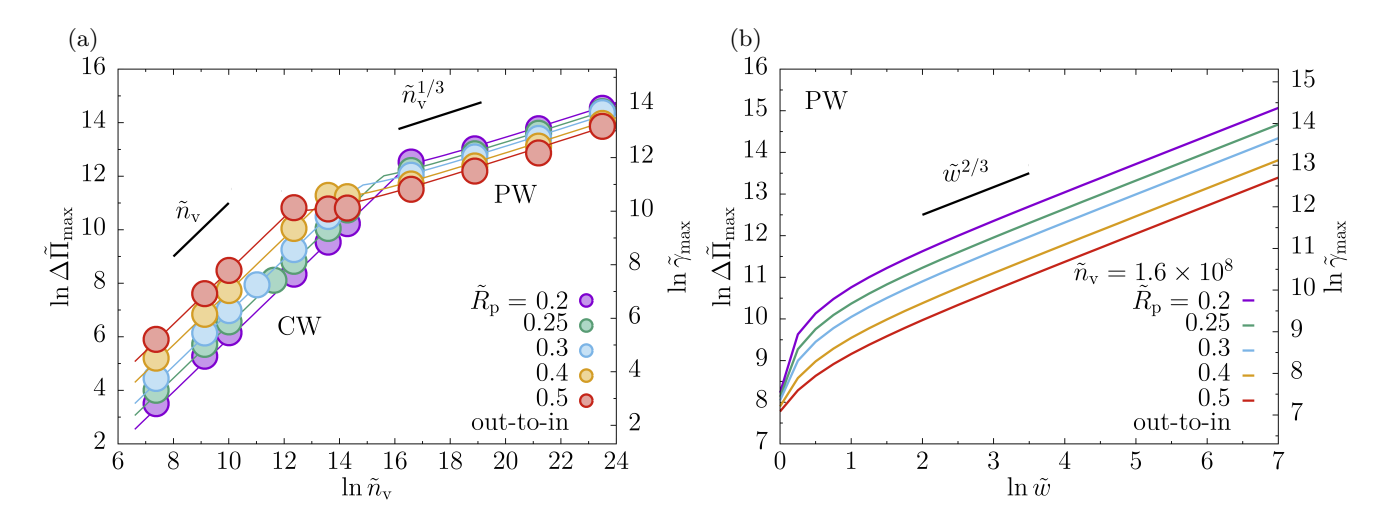


FIG. 3. Maximal reduced osmotic pressure difference  $\Delta \tilde{\Pi}$  and membrane tension  $\tilde{\gamma}$  for out-to-in wrapping, membrane bending rigidity  $\kappa = 50\,k_{\rm B}T$ , and various reduced particle sizes  $\tilde{R}_{\rm p}$ . (a) Data obtained using triangulated membranes (points) and a spherical-cap approximation calculations (lines), plotted as function of the reduced osmotic concentration  $\tilde{n}_{\rm v}$  for fixed reduced adhesion strength  $\tilde{w}=100$ . (b) Data obtained using pressure-only calculations plotted as function of the reduced adhesion strength  $\tilde{w}$  for fixed reduced osmotic concentration  $\tilde{n}_{\rm v}=1.6\times10^8$ .

transitions meet at the triple point,  $\tilde{w}^* = (1 + \tilde{R}_{\rm p})^2$  and  $\tilde{n}_v^* = 8\pi\kappa[(1 + \tilde{R}_{\rm p})^2 - 1]/(v - \ln v - 1)$ . For  $\tilde{n}_v > \tilde{n}_v^*$ , the binding transition at adhesion strength  $\tilde{w} = (1 + \tilde{R}_{\rm p})^2$  is continuous, as discussed for solute-free systems in Refs. [41–43, 45]. The adhesion strengths for the separate, discontinuous envelopment transition  $W_2$  can only be predicted numerically from equating the energy of a partial-wrapped state with the complete-wrapped state. The parameter regime for stable partial-wrapped states increases with increasing  $\tilde{n}_v$ , and all transitions shift to higher adhesion strengths with increasing  $\tilde{R}_{\rm p}$ .

For in-to-out wrapping, separate binding and envelopment transitions are found for all osmotic concentrations, see Fig. 2 (b). The binding transition  $W_1$  at  $\tilde{w} = (1 - \tilde{R}_p)^2$  is continuous [41–43, 45]. For low osmotic concentrations, the envelopment transition  $W_2$  at  $\tilde{w} = [1 + \tilde{R}_p/(1 - \tilde{R}_p^2)^{1/2}]^2$  is also continuous and essentially independent of the osmotic concentration [41-43, 45]. For high osmotic concentrations, the envelopment transition is discontinuous and the stability of partial-wrapped states strongly increases with increasing osmotic concentration. With increasing particle size partial-wrapped states are stabilised because the curvatures of particle and vesicle are more similar; the binding transition  $W_1$ shifts to lower and the envelopment transition  $W_2$  to higher adhesion strengths. The main difference to out-toin wrapping is the lack of a direct transition between nonwrapped and complete-wrapped states at low osmotic concentrations.

In general, the osmotic pressure difference between interior and exterior of a vesicle corresponds to a membrane tension  $\gamma = R_{\rm v}\Delta\Pi/2$  via the Young-Laplace equation. The reduced osmotic pressure-induced tension, as well as

the osmotic pressure difference,

$$\tilde{\gamma} = \frac{\Delta \tilde{\Pi}}{2} = \frac{\gamma R_{\rm v}^2}{k_B T} = \frac{3}{8\pi} \left(\frac{1}{v} - 1\right) \tilde{n}_{\rm v} \tag{4}$$

for out-to-in wrapping increase with increasing initial osmotic concentration and decreasing reduced vesicle volume v, see Fig. 2 and supporting information. For in-to-out wrapping, an analogous expression holds for  $v^*$ . For the calculation of the tension, we approximate the inhomogeneous mean curvature of the vesicle during wrapping by the mean curvature H of the initially spherical vesicle,  $H_{\rm init} = R_{\rm v}^{-1}$ .

Maximal membrane tensions for various particle-to-vesicle size ratios and osmotic concentrations during out-to-in wrapping are shown in Fig. 3. For reduced adhesion strength  $\tilde{w}=100$ , the particles are complete-wrapped for  $\tilde{n}_{\rm v}\lesssim 10^5-10^7$  and partial-wrapped for higher osmotic concentrations. Our calculations based on a spherical-cap model [57] excellently agree with our calculations using triangulated membranes, see Fig. 3 (a). For low osmotic concentrations, the maximal tension  $\gamma_{\rm max}$  (maximal osmotic pressure difference  $\Delta\Pi_{\rm max}$ ) increases linearly with increasing  $\tilde{n}_{\rm v}$ ,

$$\tilde{\gamma}_{\text{max}} = \frac{3}{8\pi} \left[ \frac{1}{(1 - \tilde{R}_{p}^{2})^{3/2} - \tilde{R}_{p}^{3}} - 1 \right] \tilde{n}_{v}.$$
 (5)

For the high osmotic concentrations, Figs. 3 (a) and (b) display power laws of  $\Delta \tilde{\Pi}_{max}$  and  $\Delta \tilde{\gamma}_{max}$ , both as functions of  $\tilde{n}_{v}$  and  $\tilde{w}$ . These power laws are very well captured by a high-pressure/small-wrapping approximation, see supporting information,

$$\tilde{\gamma}_{\text{max}} = \left(\frac{3\kappa\tilde{w}}{2k_{\text{B}}T}\right)^{2/3} \tilde{R}_{\text{p}}^{-1} \left(\tilde{R}_{\text{p}} + 1\right)^{-1/3} \left(\frac{\tilde{n}_{\text{v}}}{\pi}\right)^{1/3} . \quad (6)$$

The increase of the maximal tension with osmotic concentration is weaker compared with low osmotic concentrations because the wrapping fractions of the partial-wrapped particles decrease with increasing  $\tilde{n}_{\rm v}$ .

Wrapping-induced osmotic pressure difference and membrane tension for many-particle wrapping can significantly increase the particle-induced membrane tension. Using a small-wrapping approximation, we predict the minimum number of particles

$$N_{\mathrm{p},\ell} = \frac{64\pi\gamma_{\ell}^{3}V_{0}^{2}}{3\tilde{n}_{\mathrm{v}}k_{B}Tw^{2}}\left[\frac{3}{A_{\mathrm{v}}A_{\mathrm{p}}} + \frac{1}{2\pi V_{0}}\left(\frac{1}{R_{\mathrm{p}}} + \frac{1}{R_{\mathrm{v}}}\right)\right]\;. \eqno(7)$$

to exceed a threshold tension  $\gamma_\ell$  for out-to-in wrapping, e.g. the lipid-bilayer lytic tension. For in-to-out wrapping, the same power-law dependence  $N_{\rm p,\ell} \propto w^{-2}$  is found, see supporting information. Figure 4 shows the number of particles required for lysis for physiological osmotic concentration, strong adhesion, threshold tension  $\gamma_\ell = 2.5 \, k_{\rm B} T/{\rm nm}^2$ , and various particle and vesicle radii. Because of the cubic dependence on  $\gamma_\ell$ , the predicted values for  $N_{\rm p,\ell}$  are very different for  $\gamma_\ell = 1.3 \, k_{\rm B} T/{\rm nm}^2$  for MscS activation [27],  $\gamma_\ell = 2.5 \, k_{\rm B} T/{\rm nm}^2$  for MscL activation and for the lytic tension for vesicles made of purified endoplasmic reticulum membrane [28, 59], and  $\gamma_\ell = 6 \, k_{\rm B} T/{\rm nm}^2$  for the lytic tension of dioleoylphosphatidylcholine (DOPC) vesicles [60].

For biological cells under physiological conditions, the Gibbs-Donnan equilibrium determines the intracellular ion concentrations. Negatively charged (large) proteins within the cell, for which the membrane is impermeable, and active ion transport across the membrane play a dominant role. Mechanosensitive channels open when the membrane tension exceeds a threshold value (below the lytic tension). They allow for the exchange of ions and small proteins, relieve a high internal osmotic concentration, and avoid membrane rupture and guarantee cell viability. However, this depends strongly on environmental conditions. Channel opening has been shown to protect bacteria from an osmotic shock after exposure to a hypotonic solution [61]. On the contrary, for cells suspended in isotonic solution with low protein concentration, the breakdown of physiological regulation mechanisms for the intracellular ion concentration for open channels can cause lysis due to high internal protein-induced pressures. An example for this effect is red blood cells in suspension in a low protein content, where nanoparticles can induce hemolysis [62].

For a spherical particle with radius  $R_{\rm p} \approx 50\,{\rm nm}$  that approximates the volume of a T4 phage [63], and a spherical vesicle with radius  $R_{\rm p} \approx 680\,{\rm nm}$  that approximates the volume of *E.coli* [64], Fig. 4 shows that our calculations predict activation of mechanosensitive channels

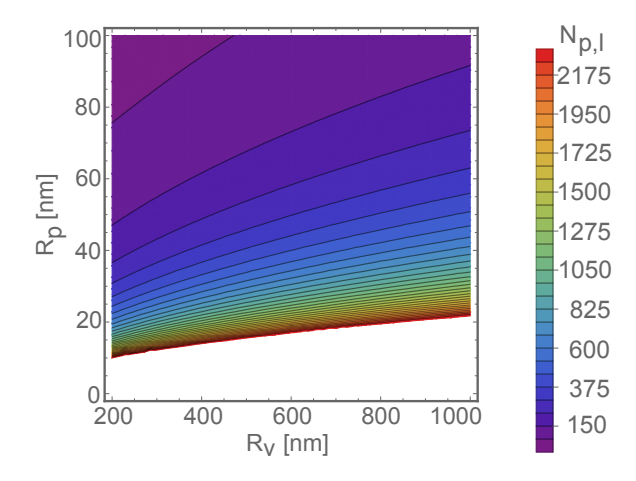


FIG. 4. Minimal number of particles required for vesicle lysis for various radii of particle and vesicle for out-to-in wrapping. The calculations have been performed at physiological solute concentration of 308 mOsm/l, for a particle-membrane adhesion strength  $w = 0.66 k_B T/\text{nm}^2$ , and a lytic membrane tension  $\gamma_{\ell} = 2.5 k_B T/\text{nm}^2$ .

for only few hundred phages. We predict  $N_{\rm p,\ell} \approx 300$  for opening MscL channels and  $N_{\rm p,\ell} \approx 50$  for opening MscS channels [27, 28]. Interestingly, even though we neglect a turgor pressure prior to wrapping, our predictions are similar to the "burst sizes" that have been reported for E.coli [65, 66]. For red blood cells with activated mechanosensitive channels, we estimate because of the excluded volume of the hemoglobin molecules aloneusing the Carnahan-Starling equation of state—a membrane tension  $> 6 \, k_B T/{\rm nm}^2$  that can lead to hemolysis.<sup>3</sup>

Our finite osmotic-concentration model includes a mechanism that maintains the volume of vesicles and cells, which is vital for the generation of tension in closed compartments bounded by fluid membranes. A somewhat similar system to nanoparticle binding to vesicles is the adhesion of bacteria to a surface with a dense, regular array of nanopillars. Here, theoretical calculations for planar membranes predict high, adhesion-induced membrane tension and therefore rupture in-between the pillars [67]. In general, nanomaterial-adhesion induced lysis can be expected for all cells that cannot regulate membrane area, such as bacteria and red blood cells. Mammalian cells are often equipped with tension-regulation mechanisms that replenish the lipids in the membrane if the tension increases, e.g. by disassembling caveolae [68]. This can prevent nanoparticle wrapping-induced lysis. For example, in toxicological tests, human dermal fibroblasts were not affected by gold nanoparticles that had antibacteriocidal effects [38]. However, in mammalian cells nanoparticle adhesion-induced tension may induce lyso-

<sup>&</sup>lt;sup>2</sup> A particle-membrane adhesion strength  $w=0.66\,k_BT/\mathrm{nm}^2$  can be expected for dense packing of receptor-ligand bonds and for silica particles at DMPC bilayers [43, 58].

<sup>&</sup>lt;sup>3</sup> Red blood cells contain  $\approx 2.7 \times 10^8$  hemoglobin molecules per cell with a volume fraction > 25 %, and have a membrane area of  $\approx 140 \, \mu \text{m}^2$ . The volume of healthy, discocytic cells is  $\approx 100 \, \mu \text{m}^3$ .

somal damage and eventually lead to cell death after the nanoparticles have passed the plasma membrane [69].

We have predicted wrapping phase diagrams for spherical nanoparticles at vesicles with finite osmotic concentration, wrapping-induced membrane tension, and for reaching a threshold tension as for wrapping-induced vesicle lysis. Our numerical modelling approach that includes osmotic pressure can be readily applied to other membrane-bounded compartments and to nanomaterials with different shapes, such as ellipsoidal or cylindrical nanoparticles. The extension of our calculations to multicomponent cell membranes [70], membranes with spontaneous curvature [43], membranes supported by a cortical cytoskeletal network with shear elasticity [71], membranes coupled to active cytoskeletal forces [72], and to systems with membrane-mediated clustering of nanoparticles [73, 74], can be next steps toward quantifying the importance of osmotic pressure for cells in vivo.

### ASSOCIATED CONTENT

## **Supporting Information**

This material is available free of charge on the ACS Publications website at DOI: XXX.

Details of the analytical calculations. Numerical results for reduced vesicle deformation energies, reduced volumes, and reduced osmotic pressure differences as function of particle wrapping fraction. Estimate of excess area due to membrane fluctuations. Discussion of energy barriers for discontinuous transitions. Additional evaluations for osmotic pressure difference and membrane tension for varying osmotic concentration, adhesion strength, particle radius, and membrane bending rigidity for out-to-in and in-to-out wrapping. Minimal

particle numbers for vesicle lysis for in-to-out wrapping. (PDF)

### **AUTHOR INFORMATION**

### Corresponding Authors

Thorsten Auth (t.auth@fz-juelich.de) and Gerhard Gompper (g.gompper@fz-juelich.de).

#### **Author Contributions**

S. Dasgupta, T. Auth, and G. Gompper designed the research. Q. Yu, S. Dasgupta, and T. Auth developed the numerical calculations. Q. Yu performed the triangulated-membrane calculations and analyzed the data; S. Dasgupta contributed code for the analysis. T. Auth performed the analytical pressure-only calculations. Q. Yu, T. Auth, and G. Gompper discussed the results and wrote the manuscript.

#### Notes

The authors declare no competing financial interest.

### ACKNOWLEDGMENTS

We thank K. Brakke (Selinsgrove, PA) for advice on Surface Evolver and for helpful discussions on numerical techniques. We thank V. Lobaskin (Dublin) for helpful discussions. Support from the EU FP7 NMP collaborative project PreNanoTox (309666) is gratefully acknowledged. QY acknowledges support from the China Scholarship Council (CSC).

Dasgupta, S.; Auth, T.; Gompper, G. J. Phys.: Condens. Matter 2017, 29, 373003.

<sup>[2]</sup> Dufort, S.; Sancey, L.; Coll, J.-L. Adv. Drug Delivery Rev. 2012, 64, 179–189.

<sup>[3]</sup> Cho, E. C.; Zhang, Q.; Xia, Y. Nat. Nanotech. **2011**, 6, 385–391.

<sup>[4]</sup> Champion, J. A.; Katare, Y. K.; Mitragotri, S. Proc. Natl. Acad. Sci. U.S.A. 2007, 104, 11901–11904.

<sup>[5]</sup> Park, J.-G.; Forster, J. D.; Dufresne, E. R. J. Am. Chem. Soc. 2010, 132, 5960-5961.

<sup>[6]</sup> Weir, A.; Westerhoff, P.; Fabricius, L.; Hristovski, K.; Von Goetz, N. Environ. Sci. Technol. 2012, 46, 2242–2250.

<sup>[7]</sup> McHale, G.; Newton, M. I. Soft Matter 2011, 7, 5473– 5481.

<sup>[8]</sup> Wright, S. L.; Kelly, F. J. Environ. Sci. Technol. 2017, 51, 6634–6647.

<sup>[9]</sup> Alimi, O. S.; Farner Budarz, J.; Hernandez, L. M.; Tufenkji, N. Environ. Sci. Technol. 2018, 52, 1704–1724.

<sup>[10]</sup> Ahamed, M.; AlSalhi, M. S.; Siddiqui, M. Clin. Chim. Acta. 2010, 411, 1841–1848.

<sup>[11]</sup> Hoet, P. H.; Brüske-Hohlfeld, I.; Salata, O. V. J. Nanobiotechnol. 2004, 2, 12.

<sup>[12]</sup> Pissuwan, D.; Valenzuela, S. M.; Cortie, M. B. Biotechnol. Genet. Eng. Rev. 2008, 25, 93–112.

<sup>[13]</sup> Xu, L.; Kuang, H.; Wang, L.; Xu, C. J. Mater. Chem. 2011, 21, 16759–16782.

<sup>[14]</sup> Xu, C.; Sun, S. Adv. Drug Delivery Rev. 2013, 65, 732–743.

<sup>[15]</sup> Maier-Hauff, K.; Ulrich, F.; Nestler, D.; Niehoff, H.; Wust, P.; Thiesen, B.; Orawa, H.; Budach, V.; Jordan, A. J. Neuro-Oncol. 2011, 103, 317–324.

<sup>[16]</sup> Saraiva, C.; Praça, C.; Ferreira, R.; Santos, T.; Ferreira, L.; Bernardino, L. J. Controlled Release 2016, 235, 34–47.

- [17] Guan, L.; Rizzello, L.; Battaglia, G. Nanomed. 2015, 10, 2757–2780.
- [18] Ferguson, S. W.; Nguyen, J. J. Controlled Release 2016, 228, 179–190.
- [19] Melo, S. A.; Luecke, L. B.; Kahlert, C.; Fernandez, A. F.; Gammon, S. T.; Kaye, J.; LeBleu, V. S.; Mittendorf, E. A.; Weitz, J.; Rahbari, N., et al. *Nature* 2015, 523, 177.
- [20] Werner, M.; Auth, T.; Beales, P. A.; Fleury, J. B.; Höök, F.; Kress, H.; Van Lehn, R. C.; Müller, M.; Petrov, E. P.; Sarkisov, L., et al. *Biointerphases* 2018, 13, 028501.
- [21] Nel, A. E.; Mädler, L.; Velegol, D.; Xia, T.; Hoek, E. M.; Somasundaran, P.; Klaessig, F.; Castranova, V.; Thompson, M. Nat. Mater. 2009, 8, 543.
- [22] Rauch, C.; Farge, E. Biophys. J. 2000, 78, 3036–3047.
- [23] Wei, Q.; Huang, C.; Zhang, Y.; Zhao, T.; Zhao, P.; Butler, P.; Zhang, S. Adv. Mater. 2018, 1707464.
- [24] Thottacherry, J. J.; Kosmalska, A. J.; Kumar, A.; Vishen, A. S.; Elosegui-Artola, A.; Pradhan, S.; Sharma, S.; Singh, P. P.; Guadamillas, M. C.; Chaudhary, N., et al. *Nat. Commun.* 2018, 9, 4217.
- [25] Borges, R.; Travis, E. R.; Hochstetler, S. E.; Wightman, R. M. J. Biol. Chem. 1997, 272, 8325–8331.
- [26] Vorselen, D.; MacKintosh, F. C.; Roos, W. H.; Wuite, G. J. L. ACS Nano 2017, 11, 2628–2636.
- [27] Sukharev, S. Biophys. J. 2002, 83, 290–298.
- [28] Chiang, C.-S.; Anishkin, A.; Sukharev, S. Biophys. J. 2004, 86, 2846–2861.
- [29] Sukharev, S. I.; Sigurdson, W. J.; Kung, C.; Sachs, F. J. Gen. Physiol. 1999, 113, 525–540.
- [30] De Belly, H.; Jones, P. H.; Paluch, E. K.; Chalut, K. J. bioRxiv 2019, 798959.
- [31] Hajipour, M. J.; Fromm, K. M.; Ashkarran, A. A.; de Aberasturi, D. J.; de Larramendi, I. R.; Rojo, T.; Serpooshan, V.; Parak, W. J.; Mahmoudi, M. Trends Biotechnol. 2012, 30, 499–511.
- [32] Sondi, I.; Salopek-Sondi, B. J. Colloid Interface Sci. 2004, 275, 177–182.
- [33] Hasan, J.; Crawford, R. J.; Ivanova, E. P. Trends Biotechnol. 2013, 31, 295–304.
- [34] Ivanova, E. P.; Hasan, J.; Webb, H. K.; Gervinskas, G.; Juodkazis, S.; Truong, V. K.; Wu, A. H.; Lamb, R. N.; Baulin, V. A.; Watson, G. S., et al. *Nat. Commun.* 2013, 4.
- [35] Lin, N.; Berton, P.; Moraes, C.; Rogers, R. D.; Tufenkji, N. Adv. Colloid Interface Sci. 2018, 252, 55– 68.
- [36] Paracini, N.; Clifton, L. A.; Skoda, M. W.; Lakey, J. H. Proc. Natl. Acad. Sci. U.S.A. 2018, 115, E7587–E7594.
- [37] Mohamed, M. M.; Fouad, S. A.; Elshoky, H. A.; Mohammed, G. M.; Salaheldin, T. A. Int. J. Veterinary Sci. Med. 2017, 5, 23–29.
- [38] Penders, J.; Stolzoff, M.; Hickey, D. J.; Andersson, M.; Webster, T. J. Int. J. Nanomed. 2017, 12, 2457.
- [39] Shamaila, S.; Zafar, N.; Riaz, S.; Sharif, R.; Nazir, J.; Naseem, S. Nanomater. 2016, 6, 71.
- [40] Huh, A. J.; Kwon, Y. J. J. Controlled Release 2011, 156, 128–145.
- [41] Yu, Q.; Othman, S.; Dasgupta, S.; Auth, T.; Gompper, G. Nanoscale 2018, 10, 6445-6458.
- [42] Bahrami, A. H.; Lipowsky, R.; Weikl, T. R. Soft Matter 2016, 12, 581–587.

- [43] Agudo-Canalejo, J.; Lipowsky, R. ACS Nano 2015, 9, 3704–3720.
- [44] Liu, J.; Kaksonen, M.; Drubin, D. G.; Oster, G. Proc. Natl. Acad. Sci. U.S.A. 2006, 103, 10277–10282.
- [45] Agudo-Canalejo, J.; Lipowsky, R. Nano Lett. 2015, 15, 7168–7173.
- [46] Reimhult, E.; Hoeoek, F.; Kasemo, B. Langmuir 2003, 19, 1681–1691.
- [47] Jackman, J. A.; Choi, J.-H.; Zhdanov, V. P.; Cho, N.-J. Langmuir 2013, 29, 11375–11384.
- [48] Oglkecka, K.; Rangamani, P.; Liedberg, B.; Kraut, R. S.; Parikh, A. N. *eLife* **2014**, 3, e03695.
- [49] Kroll, D.; Gompper, G. Science 1992, 255, 968.
- [50] Gompper, G.; Kroll, D. M. J. Phys.: Condens. Matter 1997, 9, 8795.
- [51] Sunil Kumar, P. B.; Gompper, G.; Lipowsky, R. Phys. Rev. Lett. 2001, 86, 3911–3914.
- [52] Gompper, G.; Kroll, D. M. In Statistical Mechanics of Membranes and Surfaces; Nelson, D. R., Piran, T., Weinberg, S., Eds.; World Scientific: Singapore, 2004.
- [53] Brakke, K. A. Exp. Math. 1992, 1, 141–165.
- [54] Helfrich, W.; Servuss, R.-M. Nuovo Cimento D 1984, 3, 137–151.
- [55] Dasgupta, S.; Auth, T.; Gompper, G. Nano Lett. 2014, 14, 687–693.
- [56] Deserno, M. Phys. Rev. E 2004, 69, 031903.
- [57] Lipowsky, R. Biophys. J. 1993, 64, 1133–1138.
- [58] Moy, V. T.; Jiao, Y.; Hillmann, T.; Lehmann, H.; Sano, T. Biophys. J. 1999, 76, 1632–1638.
- [59] Upadhyaya, A.; Sheetz, M. P. Biophys. J. 2004, 86, 2923–2928.
- [60] Portet, T.; Dimova, R. Biophys. J. 2010, 99, 3264–3273.
- [61] Levina, N.; Tötemeyer, S.; Stokes, N. R.; Louis, P.; Jones, M. A.; Booth, I. R. EMBO J. 1999, 18, 1730– 1737.
- [62] Dobrovolskaia, M. A.; Clogston, J. D.; Neun, B. W.; Hall, J. B.; Patri, A. K.; McNeil, S. E. Nano Lett. 2008, 8, 2180–2187.
- [63] Fokine, A.; Chipman, P. R.; Leiman, P. G.; Mesyanzhinov, V. V.; Rao, V. B.; Rossmann, M. G. Proc. Natl. Acad. Sci. U.S.A. 2004, 101, 6003–6008.
- [64] Milo, R.; Phillips, R. Cell biology by the numbers; Garland Science, 2015.
- [65] Hadas, H.; Einav, M.; Fishov, I.; Zaritsky, A. Microbiol. 1997, 143, 179–185.
- [66] Delbrück, M. J. Bacteriol. 1945, 50, 131.
- [67] Pogodin, S.; Hasan, J.; Baulin, V. A.; Webb, H. K.; Truong, V. K.; Nguyen, T. H. P.; Boshkovikj, V.; Fluke, C. J.; Watson, G. S.; Watson, J. A., et al. *Biophys. J.* 2013, 104, 835–840.
- [68] Sinha, B.; Köster, D.; Ruez, R.; Gonnord, P.; Bastiani, M.; Abankwa, D.; Stan, R. V.; Butler-Browne, G.; Vedie, B.; Johannes, L., et al. Cell 2011, 144, 402–413.
- [69] Wang, F.; Yu, L.; Monopoli, M. P.; Sandin, P.; Mahon, E.; Salvati, A.; Dawson, K. A. Nanomed. Nanotechnol. Biol. Med. 2013, 9, 1159–1168.
- [70] Curk, T.; Wirnsberger, P.; Dobnikar, J.; Frenkel, D.; Saric, A. Nano Lett. 2018, 18, 5350–5356.
- [71] Dumitru, A. C.; Poncin, M. A.; Conrard, L.; Dufrêne, Y. F.; Tyteca, D.; Alsteens, D. Nanoscale Horiz. 2018, 3, 293–304.
- [72] Fošnarič, M.; Penič, S.; Iglič, A.; Kralj-Iglič, V.; Drab, M.; Gov, N. Soft Matter 2019, 15, 5319–5330.

[73] Idema, T.; Kraft, D. J. Curr. Opin. Colloid Interface Sci.  ${f 2019},\ 40,\ 58-69.$ 

[74] Bahrami, A. H.; Weikl, T. R. Nano Lett. 2018, 18, 1259– 1263.